The use of DBD plasma treatment and polymerization for the enhancement of biomedical UHMWPE

By Pieter Cools, Stijn Van Vrekhem, Nathalie De Geyter and Rino Morent

P. Cools, Dr. N. De Geyter, Prof. Dr. R. Morent

Research Unit Plasma Technology (RUPT), Department of Applied Physics, Faculty of Engineering, Ghent University, St-Pietersnieuwstraat 41 B4, Ghent, 9000, Belgium

E-mail: Pieter.cools@ugent.be

Tel: +32 9 264 38 38

The use of DBD plasma treatment and polymerization for the enhancement of biomedical UHMWPE

Pieter Cools*, Stijn Van Vrekhem, Nathalie De Geyter, Rino Morent

P. Cools, S. Van Vrekhem, Dr. N. De Geyter, Prof. Dr. R. Morent

Research Unit Plasma Technology (RUPT), Department of Applied Physics, Faculty of Engineering, Ghent University, St-Pietersnieuwstraat 41 B4, Ghent, 9000, Belgium

E-mail: Pieter.cools@ugent.be

Abstract

Surface modification of polymers for biomedical applications is a thoroughly studied area. The goal of this paper is to show the use of atmospheric pressure plasma technology for the treatment of polyethylene shoulder implants. Atmospheric pressure plasma polymerization of methyl methacrylate will be performed on PE samples to increase the adhesion between the polymer and a PMMA bone cement. For the plasma polymerization, a dielectric barrier discharge is used, operating in a helium atmosphere at ambient pressure. Parameters such as treatment time, monomer gas flow and discharge power are varied one at a time. Chemical and physical changes at the sample surface are studied making use of X-ray photoelectron spectroscopy and atomic force microscopy measurements. Coating thicknesses are determined by making use of optical reflectance spectroscopy. After characterization, the coated samples are incubated into a phosphate buffered saline solution for a minimum of one week at 37°C, testing the coating stability when exposed to implant conditions. The results show that PMMA coatings can be deposited with a high degree of control in terms of chemical composition and layer thickness

Keywords: Dielectric barrier discharge, XPS, plasma activation, plasma polymerization, PMMA

1. Introduction

Total shoulder arthroplasty (TSA) is the third most common arthroplasty in the world.[1] It is a commonly used treatment for diseases of the glenohumeral joint, such as advanced osteoarthritis, rheumatoid arthritis or avascular necrosis.[2] An anatomical TSA mimics the anatomy of the shoulder joint and therefore consists of a humeral and glenoid component. The humeral component contains a stem and a rounded head or ball, usually made out of titanium or cobalt-chromium. The glenoid component is a concave socket made of ultra-high molecular weight polyethylene (UHMWPE). The major problem concerning total shoulder replacement today is the loosening of these components.[3] Literature states that loosening of the glenoid component is occurring more frequently than loosening of the humeral component.[1, 3] The fixation of both components has initially been performed by using a bone cement, usually a polymethyl methacrylate (PMMA) resin. Nowadays, next to bone cement fixation, also metal-backed glenoid components are used. These components are based on bone ingrowth fixation and do not need bone cement.[4] However, in spite of these metal-backed components and the fact that the glenoid component can come in different geometrical designs, e.g. pegged or keeled, the incidence of glenoid component loosening is still too high. This is mostly due to the nature of the material that is used. Although UHMWPE has adequate mechanical properties, it is an inert and non-polar material. Therefore, it is difficult to chemically bind UHMWPE in order to get an adhesive fixation.[5] Improving the adhesive properties of medical grade UHMWPE by means of surface modification could consequently lead to an improved performance of a shoulder prosthesis. Literature shows that research is going into ameliorating the adhesive properties of UHMWPE by using, amongst others, radiation methods, gas-phase based treatments or simple mechanical abrasion. Radiation methods include ion-, gamma- or electron irradiation. Gas-

phase based treatments include UV/ozone treatment, corona treatment or glow discharge treatment. [5, 6]

In the past, extensive research, using plasma activation, has been successfully done on the improvement of the wettability of polymer surfaces.[7-14] Functional groups, such as hydroxyls and alkanoates, are introduced onto the surface, making it more polar and less inert. The introduction of these functional groups occurs through a two-step process. Starting with the formation of free radicals on the polymer surface during the plasma treatment, it is followed by the reaction of these free radicals with the medium that is present. [15-19] Past research has shown that the increase in wettability can lead to an increase in cell adhesion and proliferation. [12, 20, 21]

Next to plasma activation, also plasma polymerization is an interesting technique to change the properties of a material's surface. Plasma polymerization is an easy method to produce polymer nano-films on a substrate. These plasma polymerized films are pinhole-free, completely amorphous, insolvable in most solvents and highly cross-linked, which results in a good thermal, chemical and mechanical stability. Plasma polymers also have a strong adherence on numerous substrates.[17-19, 22]

The aim of this study is to use both plasma treatment and plasma polymerization of methyl methacrylate (MMA) on an UHMWPE surface to improve its bioactivity and adhesive properties. As mentioned before, plasma treatment will turn an inert UHMWPE surface into an activated surface. Plasma polymerization of MMA will deposit a plasma-PMMA layer on the pre-activated UHMWPE surface. Since this intermediate layer then consists of the same material as the bone cement that is used in TSAs, the adhesion between the implant material and the bone cement should be improved. Both plasma activation and plasma polymerization are performed by using a dielectric barrier discharge (DBD) at medium pressure and

atmospheric pressure respectively. DBDs are known for their easy formation of a stable discharge and their scalability. The efficiency of medium pressure DBDs has already been demonstrated [9-12, 14, 23-25]. The fact that the polymerization process can be performed at atmospheric conditions highlights its simplicity.[26, 27] In order to get an insight in the modifications made to the surface, a varied set of surface analysis techniques are used. Hence, for both plasma methods, static water contact angle goniometry (WCA), Fourier transform infrared spectroscopy (FT-IR), X-ray photoelectron spectroscopy (XPS), atomic force microscopy (AFM) and optical reflectance spectroscopy (OPS) are performed.

2. Materials and methods

2.1.Chemicals and films

MMA (99%, 30 ppm MEHQ as inhibitor) was purchased from Sigma-Aldrich and used as such. Helium, dry air, argon and nitrogen (Alphagaz 1) were purchased from Air Liquide. The salts used to make the PBS solution(sodium chloride (99.8%), potassium chloride (99%), sodium hydrogenphosphate (98%), potassium dihydrogenphosphate (98%) and sodium azide (99%)) were purchased from Carl Roth and mixed to a pH of 7.4. A roll of UHMWPE film with a thickness of 0.5 mm was ordered from Goodfellow Cambridge UK. Samples of 1 cm^2 were cut out for treatment.

2.2.Plasma methods

All plasma treatments presented in this paper are performed with a dielectric barrier discharge (DBD) reactor, which is schematically presented in **Fig. 1**. The discharge is generated between two circular copper electrodes (Ø: 65 mm), which are both covered with a glass plate. The gas gap between these glass plates is 7 mm. The upper electrode is connected to a 50 kHz AC high voltage source, while the lower electrode is connected to earth through a resistor R (50 Ω) or a capacitor C (10 nF). After fixing the UHMWPE sample on the lower

glass plate using double sided tape, the plasma reactor is pumped to 0.1 kPa using a rotary vane pump and subsequently filled with the gas of choice at 3 slm (standard litre per minute). After reaching sub-atmospheric pressure (90 kPa), the plasma reactor is flushed at 3 slm with the working gas for 3 min to obtain a controllable gas composition. After this purging step, the pressure in the plasma reactor is lowered to 5.0 kPa. At this medium pressure, plasma activation is performed with a gas flow of 1 slm and for various treatment times ranging from 0 s to 1 min, as shown in **Table I**.

Plasma polymerization is done on the pre-activated UHMWPE substrates in a second DBD reactor, as monomer contamination during the activation step has to be avoided and is schematically presented in **Fig. 2**. The discharge is generated between two circular copper electrodes (Ø: 55 mm), which are both covered with a glass plate. The gas gap between these glass plates is 3.5 mm. The upper electrode is connected to a 50 kHz AC high voltage source, while the lower electrode is connected to earth through a resistor R (50 Ω) or a capacitor C (10 nF). After fixing the UHMWPE sample on the lower glass plate using double sided tape, the plasma reactor is pumped to 0.1 kPa using a rotary vane pump and subsequently filled with He at 3 slm. After reaching atmospheric pressure (100 kPa) the reactor is flushed at 3 slm with He for 3 min to obtain a controllable gas composition. After the purging step, a mixture of He and monomer gas is allowed to flow between the two electrodes. The main He flow is controlled using a mass flow controller (MKS Instruments, the Netherlands) and is adjustable in the range between 0-10 slm. The monomer is introduced in the gas chamber using a glass bubbler containing the MMA monomer, carried by a secondary He flow. The monomer flow is also controlled by a mass flow controller (MKS Instruments, the Netherlands) and has a range between 0 and 500 ml/min. For the purpose of comparison, the total gas flow is maintained at 3 slm. In the following series of experiments, the discharge power is kept constant at 30 W, while both treatment time as well as monomer concentrations

are varied. For each monomer concentration – 50, 75, 100, 125 ml/min – the treatment time is varied between 1 and 5 minutes, using intervals of 1 minute.

2.3. Electrical characterization

The DBD is electrically characterised by measuring the applied high voltage and the resultant discharge current. The high voltage applied to the upper copper electrode is measured using a 1000:1 high voltage probe (Tektronix P6015A), whereas for the monitoring of the discharge current, the voltage is measured across a 50 Ω resistor, connected in series with the discharge reactor to the ground. The obtained waveforms are recorded using a digital oscilloscope (Picoscope 3204A) and are visualized and analysed using the included software (Picoscope 6) [11]. **Fig. 3** shows the Volt – current plots of the discharge for the DBDs sustained in the four different gasses used for plasma activation and the one used for plasma polymerization. With the exception of the Ar discharge, all plasma for activation are characterized by a filamentary discharge. The Ar discharge and the He polymerization discharge are situating themselves between a glow and filamentary regime, giving only cause to a few wide peaks superimposed onto the capacitive current, guaranteeing a more homogeneous treatment and polymer deposition of the sample. The resistor in the set-up can be replaced by a capacitor of 10 nF and the voltage across this capacitor is then proportional to the charge stored on the electrodes. This latter measurement is widely used to obtain voltage versus charge plots, which form Lissajous figures. This figure is used to determine the discharge power, since the electrical energy consumed per voltage cycle is equal to the area enclosed by the Lissajous figure [28]. The discharge power P is then calculated by multiplying the electrical energy with the frequency of the feeding voltage (50 kHz) [28]. The applied discharge power is summarized in **Table I** and is slightly different for each gas. To enable an objective comparison between both plasma treatments, the results will be presented as a function of

energy density [J/cm^2]. This value is calculated by multiplying the plasma exposure time with the plasma power divided by the area of the electrodes and can also be found in **Table I**.

2.4.Surface analysis techniques

Static contact angle

The static contact angles of the treated samples are obtained at room temperature, using a commercial Krüss Easy Drop system (Krüss Gmbh, Germany) within 5 minutes after the treatment. In this paper, drops of distilled water with a volume of 1.0 µL are used as test liquid. The contact angle values, shown in this work, are obtained using Laplace-Young curve fitting and are the average of 4 values measured over an extended area of the treated samples.

XPS

XPS surface analysis of the UHMWPE samples is performed on a PHI Versaprobe II spectrometer employing a monochromatic Al K_α X-ray source ($h\nu$ = 1486.6 eV) operating at 23.3 W. All measurements were conducted in a vacuum of at least 10^{-6} Pa and the photoelectrons were detected with a hemispherical analyser positioned at an angle of 45° with respect to the normal of the sample surface. Survey scans and individual high resolution spectra (O1s and C1s) were recorded with a pass energy of 117.4 eV and 29.35 eV respectively. Elements present on the UHMWPE surfaces were identified from XPS survey scans, measuring 3 samples, with 3 points per sample and quantified with Multipak software using a Shirley background and applying the relative sensitivity factors supplied by the manufacturer of the instrument. Multipak software is also used to curve fit the high resolution C1s peaks. The hydrocarbon component of the C1s spectrum (285.0 eV) is used to calibrate the energy scale. In a next step, the peaks are deconvoluted using Gaussian–Lorentzian peak shapes and the full-width at half maximum (FWHM) of each line shape is constrained below 1.8 eV.

FT-IR

FT-IR analysis is performed on the UHMWPE samples making use of a Bruker Tensor 27 (Bruker) spectrometer equipped with a single reflection ATR accessory (MIRacle^{TM}, Pike technology) using a germanium crystal as internal reflection element. The FT-IR spectra are recorded using an MCT-detector (liquid N_2 cooled) with a resolution of 4 cm^{-1} and 32 scans are made for each sample.

OPS

Optical reflectance spectroscopy is done on silicon wafers (Siegert Wafers) making use of a Filmetrics F20 (Filmetrics) device. A fitting of an acrylic on SiO_2 is used, with air as medium. For each condition, 3 samples are measured, with 3 points per sample respectively. Only measurements with a fit over 95% are used.

AFM

In addition to chemical characterisation, the UHMWPE surface topography and roughness are also examined using an XE-70 atomic force microscope (Park Systems). 35 µm scans are recorded in non-contact mode with a silicon cantilever (Nanosensors^{TM} PPP-NCHR) and XEP software is used for surface roughness analysis after the recorded images are modified with an X and Y plane auto-fit procedure. For each condition, 1 sample was measured on three different spots per sample.

3. Results and discussion

3.1. Plasma activation

Contact angle measurements

Fig. 4 gives an overview of the change in static water contact angle (WCA) of the UHMWPE in function of the energy density when treated with the 4 different plasma gasses (dry air, He, Ar and N_2). At an energy density of 0 there has been no exposure to plasma and the WCA is situated around 93°. When exposed to plasma, the WCA quickly decreases until a plateau is reached; meaning that the surface is saturated and further treatment no longer leads to further chemical modifications. The starting point of this plateau is considered to be the best set of treatment parameters for the rest of the research and are summarized in **Table II**. For each gas, the plateau is reached at a different WCA lying between 62° and 43°, which is in close agreement with the values found by Borcia *et al*. [29]. This implies that the chemical alterations caused by the plasma are different for each gas. In order to define these alterations, XPS measurements are done on the surface to identify the chemical composition.

XPS analysis

XPS survey spectra allow to determine the atomic composition of the sample surface, while the high resolution recordings of the Cs1 peaks can be fitted as described in the materials and methods section. These curve fits give insight in the different chemical bonds between carbon and oxygen introduced by the plasma as each bond has a different binding energy. For plasma activation literature agrees on the following values: 285 eV for the C-C/C-H bond, 286.7 eV for the C-O bond, 287.7 for the C=O bond and 288.9 eV for the O-C=O bonds [14]. A schematic depiction of the curve fitting can be found in **Fig. 5** (up), while the results of both the atomic composition and the curve fitting can be found in Table III**.** When taking a closer look at the atomic concentrations, the following trend can be observed: the higher the concentration of oxygen + nitrogen, the lower the contact angle. The curve fitting results in **Table III** show that between 50-75 % of the oxygen is incorporated as C-O bonds, most likely resulting in - OH groups on the surface, while the other 25-50% is incorporated as O=C-O bonds, resulting in carboxylic acids and ester groups. Even a difference of 1-2% in

oxygen incorporation can change the WCA by several degrees. By changing the energy density, the amount of incorporated functionalities can easily be varied.

AFM imaging

Non-thermal plasma are known to have an effect on surface morphology, even at low discharge powers. In order to visualise and quantify these effects, AFM measurements are performed on both treated and untreated samples. The results of these measurements are collected in **Table II.** The roughness values (R_q) of the treated samples lie significantly below the roughness value of the untreated sample. This smoothing of the samples is caused by the etching effect of the plasma [30, 31]. This etching effect also influences the WCA of the sample. As stated by Wenzel in 1936: a higher sample roughness enhances the water contact angle compared to its smoother counterpart. To put it in other words, if two samples, a rougher and a smoother one, are submitted to the same plasma treatment, the rougher sample will give cause to a lower WCA compared to the smoother sample [32, 33]. Together with the XPS analysis, this explains why the WCAs of the N_2 and Ar treated samples are lower than the other ones.

3.2.Plasma polymerization

In what follows next, the pre-activated UHMWPE samples, as described in the above paragraphs, are used as the substrates for the plasma polymerization of MMA. The introduction of functional groups on the PE surface should help anchoring the polymer film to the substrate, as previous research has proven that untreated substrates give cause to loosening of the film when screened via stability tests

Contact angle measurements

The contact angle of commercial PMMA is situated well above 70°. The plasma polymerized samples, summarized in **Table IV** give angles that lie between 75° and 85°, up to 10° higher compared to the value of conventional PMMA. This difference in WCA is most likely due to the higher cross-linking of the MMA, resulting in the loss of a number of ester-methoxyl (CH_3-O) which are being replaced by a mixture of ketones, alcohols and ethers and C-C bonds and the repositioning of these groups towards the surface, resulting in an overall less hydrophilic surface. The WCA value for the 50 ml treatments (2 minutes) lies higher compared to the other treatments. Due to the low monomer concentration, there will be a higher energy/monomer concentration ratio, resulting in a higher fragmentation. This in turn results in a more profound loss of functionalities, leading to a more hydrophobic surface [34, 35]. In what follows, XPS and FT-IR analysis will be used to identify the chemical identity of the surface of the plasma polymerized thin film and to (semi)quantify to what extent the fragmentation and crosslinking takes place within the plasma.

XPS analysis

As mentioned in the introduction, it is known from literature that plasma polymers differ from conventional polymers in a number of ways: some of these characteristics, such as the high cross-linking will reflect themselves in the XPS measurements. De Geyter et al. stated in 2009 that an increase in discharge power or a decrease in monomer concentration leads to a higher fragmentation rate of the monomer and thus a loss of functionalities [17]. The results summed up in **Table IV** confirm this statement. The O/C values of the plasma polymerized PMMA lie in general between 0.2 and 0.25, while the commercial PMMA O/C value tops that with a factor of 2, lying close to 0.4, which is the expected value based on the chemical structure of a PMMA monomer unit. This confirms that the relatively high discharge power fragments the monomer upon entering the plasma, causing a loss of oxygen and thus the ester functionality.

To quantify the loss of functionalities, again a curve fit of the C1s peak is done which can also be found in **Table IV**. Compared to the plasma activation, a different set of binding energies is agreed upon in literature: 285 eV for the C-C/C-H bond, 286 eV for the C-C=O bond, 286.9 eV for the C-O bond and 288.9 eV for the O-C=O bond [17, 36]. A general presentation of this curve fit on commercial PMMA can be found in **Fig 5** (down) and is similar to the C1s curve fit of plasma polymerised PMMA (same binding energies, different ratios). Applying this curve fitting on the commercial PMMA C1s peak is a perfect match to what is expected based on the chemical structure of a PMMA monomer unit (a perfect 1:1:1 ratio of the 3 highest energy peaks, while the last two combined give the theoretical 27.5% O as expected). The fitting ratios of the plasma polymerized PMMA thin films strongly deviate from the commercial PMMA. As the O/C values are lower, it is no surprise that the C-C peak intensity increases between 16-22 % for all conditions. For the other peaks, this leads to a decrease between 5 and 8 %. The 1:1:1 ratio found for commercial PMMA is no longer valid, as the O-C=O peak and the C-C=O at 288.7 and 286 eV respectively have been reduced more due to the plasma compared to the C-O peak at 286.9 eV. Although it is assumed that the plasma randomly attacks the functionalities and will thus reduce them equally, some of the ester functionalities are converted into ketones, ethers and alcohols. This conversion results in an increase of the C-O peak, giving cause to the change of the ratios as they are. As the monomer concentration increases, the energy/monomer decreases which results in less fragmentation. The loss of the ester functionality (O-C=O) is less profound and the decrease of the 3 peaks lies closer to the 1:1:1 ratio.

When looking at the curve fits of the 125 ml/min series, some deviating values are found. As will be discussed in more detail in the AFM section, at this monomer concentration, there is a drastic change in the growth mechanism of the polymer. This results in a different surface morphology and a different surface chemistry.

AFM imaging

AFM is an excellent analysis tool to follow the growth of the PMMA thin film on the UHMWPE substrate. **Fig. 6** gives a series of AFM images both in function of time and monomer concentration. When comparing to the first image of the series, depicting an untreated sample, the other images show that the coating grows quite homogeneously, filling up the lower regions faster, until at the end a smooth layer is completely covering the underlying sample. When the images in function of monomer concentration are analysed, it becomes clear that for the lower concentrations the underlying structure remains visible at all times, while at higher concentrations (75-125ml/min) the underlying structure gets incorporated into the deposited film. As mentioned in the XPS section, the 125 ml/min flow rate gives a completely different surface morphology compared to the other images. Whereas the lower flow rate films follow the underlying structure, the 125 ml/min series first introduces drop like structures on the surface (see Fig 6, 3 and 5 min), transforming into a smooth surface upon further treatment. In the stability analysis, the 125 ml/min has therefore been excluded. To determine the growth rate of the deposited film, AFM could be used, but the use of optical reflectance spectroscopy, as discussed in the next paragraph, gives faster and more accurate results.

Optical reflectance spectroscopy

As described in the materials and methods section, silicon wafers are used to determine the thickness of the deposited layers. The results depicted in **Fig. 7** show that for low treatment times and low monomer concentrations, there is a linear relationship between the thickness and the deposition time. Using linear regression on the results from the first 4 datapoints, the growth rate for each monomer concentration can be calculated. For the lowest monomer concentration, a growth rate of 98 nm/min is found. Increasing the monomer flow to 100

ml/min results in an increase of the growth rate to 129 nm/min. A further increase to 125 ml/min gives a growth rate of 122 nm/min (goodness of fit~92%). These growth rates for the different monomer rates show that a linear increase in monomer concentration does not lead to a linear increase in growth rate. In 2009, De Geyter et al. already proved that the W/FM (W = discharge power, F = flow rate, M = molecular weight monomer) parameter has a big influence on the deposition rate [17]. When analysing the growth rate in function of this parameter, 3 regimes can be distinguished. In a first regime, the growth rate will increase with increasing W/FM (monomer sufficient region). As the discharge power per molecule increases, extra initiation sites are formed, resulting in an increased polymerisation rate. In the second regime, the growth rate decreases with an increase in W/FM (monomer deficient region). At this point, the discharge power per monomer molecule becomes too high, resulting in fragmentation of the molecule, causing a decrease in polymerization rate. The third regime lies in between, forming a plateau in growth rate where initiation and fragmentation balance each other out. When analysing the results of **Fig. 7**, it becomes clear that for the lower monomer flow rate(75 ml/min), the system is operating in the monomer deficient regime, as an increase in monomer concentration to 100 ml/min leads to a disproportionally higher growth rate. This comes as no surprise as the discharge power of 30 W, needed for decent crosslinking, is relatively high. When further increasing to 125 ml/min, the increase is less pronounced and after more than 3 minutes of polymerization, the linear growth relation is no longer respected. It is believed that the atmosphere within the reactor is getting saturated with monomer, resulting in an increase of monomer in the plasma. Therefore, the plasma goes from a monomer deficient regime into the monomer sufficient region, resulting in a lower growth rate [17]. Together with the results from the XPS and AFM measurements this forms an indication not to go higher in monomer concentration. Due to the fact that the highest film

growth rate is found for the 100 ml/min series, this monomer concentration will be used for the stability tests.

FT-IR & stability

In order to use these thin film coatings for biomedical applications, it is important to test their stability in the human body. To do so, the human body environment is simulated, making use of a phosphate buffered saline (PBS) solution at neutral pH. FT-IR measurements are performed at predetermined time intervals between 1 and 14 days in order to detect a possible loss of functionality. As FT-IR is more sensitive to functional changes compared to XPS, it is the preferred method. To determine the differences before and after incubation, it is important to identify the most important peaks in the FT-IR spectrum (see **Fig. 8 and 9**). For pre-activated UHMWPE, there are only a few peaks of interest: the C-H stretches at 2850, 2910 and 2950 cm^{-1} and the C-H bends at 1380 and 1470 cm^{-1} (**Fig. 8**). When a plasma PMMA coating is applied, a number of extra peaks are identified as can be seen in Figure 9. The most prominent peak is the one at 1730 cm^{-1} indicating the C=O stretch of an ester. Furthermore, there is a very broad peak between 1050 and 1300 cm^{-1} originating from the C-O stretch. This peak is not as well defined as would be expected for PMMA, which is caused by the plasma polymerization, giving a big variety in the chemical surroundings of the C-O bond, causing the peak to be smeared out broadly. The same conclusion can be drawn for the C-H stretches between 2850 and 2950 cm^{-1} which are smeared out as well (**Fig 9.a**). When analysing the spectra for the different conditions (see **Fig. 9.a-c**), a number of differences can be noted. FT-IR measures over a depth of 600 nm, resulting in the thinner film spectra (shorter treatment times) being a mixture of the plasma PMMA film and the underlying UHMWPE substrate. As the coating becomes thicker, the PE peaks are engulfed by the PMMA signal. As can be deduced from **Figure 9.c**, there are some differences in the FT-IR spectra before and after incubation (14 days). The main change is the appearance of the OH stretch between 3000 and

3500 cm^{-1}. This is an indication of (partial) hydrolysis of the ester functionality. This is not a surprise, as PBS is an aqueous solution and PMMA is known to hydrolyse quite easily. Due to this hydrolysis, the carbonyl peak at 1730 cm^{-1} is less pronounced and in some cases even shifted into a second peak at 1680 cm^{-1} originating from hydrogen bonds to the carbonyl peak. Furthermore, a small peak is appearing at 975 cm^{-1} originating from the out of plane OH bend. Overall, it can be concluded that some changes can be noted before and after the incubation period, but further study has to be done to fully map the degradation and to what extend it takes place.

Conclusions

The results of this paper can be divided in two parts: plasma activation of UHMWPE on the one hand and plasma polymerization of MMA on the other hand. Both procedures have been analysed thoroughly, making use of a broad range of analysis techniques. For the plasma activation, it can be concluded that plasma is an excellent tool to enhance and fine-tune the wettability of the hydrophobic UHMWPE via the incorporation of a mix of polar groups such as alcohols, ketones and ethers. As it is a non-invasive technique, the integrity of the substrate is conserved, allowing the treatment of more delicate structures such as certain biomedical implants. The plasma activated surface forms an excellent substrate for the plasma deposition of thin films, as the activated groups guarantee a strong bond. The analysis of the plasma polymerized thin films shows that a dense, highly cross-linked film can be deposited at relatively high rates. Varying parameters such as energy density and monomer concentration enable the operator with a high amount of control over film parameters such as thickness and preservation of functional groups. AFM measurements show a homogeneous growth process, following the underlying structure of the substrate. Stability tests in PBS show that the coatings are stable in a human like environment, opening a window to biomedical applications, which will be researched in future work.

Acknowledgements

This research has received funding from the European Research Council under the European Union's Seventh Framework Program (FP/2007-2013) / ERC Grant Agreement n. 279022.

References

[1] L.A. Kaback, A. Green, T.A. Blaine, Glenohumeral arthritis and total shoulder replacement,Medicine and health, Rhode Island 95/4 (2012) 120.
[2] E.T. Ricchetti, G.R.J. Williams, Total shoulder arthroplasty: indications, technique and results,Operative Techniques in Orthopaedics 21/1 (2011) 28
[3] K.I. Bohsali, M.A. Wirth, C.A. Rockwood, Jr., Complications of total shoulder arthroplasty,The Journal of bone and joint surgery. American volume 88/10 (2006) 2279.
[4] E.J. Strauss, C. Roche, P.H. Flurin, T. Wright, J.D. Zuckerman, The glenoid in shoulder arthroplasty,Journal of shoulder and elbow surgery / American Shoulder and Elbow Surgeons ... [et al.] 18/5 (2009) 819.
[5] R. Oosterom, T.J. Ahmed, J.A. Poulis, H.E. Bersee, Adhesion performance of UHMWPE after different surface modification techniques,Medical engineering & physics 28/4 (2006) 323.
[6] A. Turos, A.M. Abdul-Kader, R. Ratajczak, A. Stonert, Modification of UHMWPE by ion, electron and gamma-ray irradiation,Vacuum 83 (2009) S54.
[7] D. Hegemann, H. Brunner, C. Oehr, Plasma treatment of polymers for surface and adhesion improvement,Nucl Instrum Meth B 208 (2003) 281.
[8] J.N. Lai, B. Sunderland, J.M. Xue, S. Yan, W.J. Zhao, M. Folkard, B.D. Michael, Y.G. Wang, Study on hydrophilicity of polymer surfaces improved by plasma treatment,Appl Surf Sci 252/10 (2006) 3375.
[9] R. Morent, N. De Geyter, J. Verschuren, K. De Clerck, P. Kiekens, C. Leys, Non-thermal plasma treatment of textiles,Surface and Coatings Technology 202/14 (2008) 3427.
[10] N. De Geyter, R. Morent, C. Leys, Surface characterization of plasma-modified polyethylene by contact angle experiments and ATR-FTIR spectroscopy,Surface and Interface Analysis 40/3-4 (2008) 608.
[11] N. De Geyter, R. Morent, T. Desmet, M. Trentesaux, L. Gengembre, P. Dubruel, C. Leys, E. Payen, Plasma modification of polylactic acid in a medium pressure DBD,Surface and Coatings Technology 204/20 (2010) 3272.
[12] T. Jacobs, N. De Geyter, R. Morent, T. Desmet, P. Dubruel, C. Leys, Plasma treatment of polycaprolactone at medium pressure,Surface and Coatings Technology 205, Supplement 2/0 (2011) S543.
[13] R. Morent, N. De Geyter, T. Desmet, P. Dubruel, C. Leys, Plasma surface modification of biodegradable polymers: a review,Plasma Processes and Polymers 8/3 (2011) 171.
[14] N. De Geyter, R. Morent, C. Leys, L. Gengembre, E. Payen, Treatment of polymer films with a dielectric barrier discharge in air, helium and argon at medium pressure,Surface and Coatings Technology 201/16 (2007) 7066.
[15] S. Teodoru, Y. Kusano, N. Rozlosnik, P.K. Michelsen, Continuous Plasma Treatment of Ultra-High-Molecular-Weight Polyethylene (UHMWPE) Fibres for Adhesion Improvement,Plasma Process Polym 6 (2009) S375.
[16] R. Morent, N. De Geyter, S. Van Vlierberghe, P. Dubruel, C. Leys, L. Gengembre, E. Schacht, E. Payen, Deposition of HMDSO-based coatings on PET substrates using an atmospheric pressure dielectric barrier discharge,Progress in Organic Coatings 64/2–3 (2009) 304.
[17] N. De Geyter, R. Morent, S. Van Vlierberghe, P. Dubruel, C. Leys, L. Gengembre, E. Schacht, E. Payen, Deposition of polymethyl methacrylate on polypropylene substrates using an atmospheric pressure dielectric barrier discharge,Progress in Organic Coatings 64/2 (2009) 230.
[18] R. Morent, N. De Geyter, S. Van Vlierberghe, E. Vanderleyden, P. Dubruel, C. Leys, E. Schacht, Deposition of polyacrylic acid films by means of an atmospheric pressure dielectric barrier discharge,Plasma Chemistry and Plasma Processing 29/2 (2009) 103.
[19] N. De Geyter, R. Morent, S. Van Vlierberghe, M. Frere-Trentesaux, P. Dubruel, E. Payen, Effect of electrode geometry on the uniformity of plasma-polymerized methyl methacrylate coatings,Progress in Organic Coatings 70/4 (2011) 293.

[20] Y. Arima, H. Iwata, Effect of wettability and surface functional groups on protein adsorption and cell adhesion using well-defined mixed self-assembled monolayers,Biomaterials 28/20 (2007) 3074.
[21] C. Lucchesi, B.M. Ferreira, E.A. Duek, A.R. Santos, Jr., P.P. Joazeiro, Increased response of Vero cells to PHBV matrices treated by plasma,Journal of materials science. Materials in medicine 19/2 (2008) 635.
[22] F. Benitez, E. Martinez, J. Esteve, Improvement of hardness in plasma polymerized hexamethyldisiloxane coatings by silica-like surface modification,Thin Solid Films 377 (2000) 109.
[23] N. De Geyter, R. Morent, L. Gengembre, C. Leys, E. Payen, S. Van Vlierberghe, E. Schacht, Increasing the hydrophobicity of a PP film using a helium/CF4 DBD treatment at atmospheric pressure,Plasma Chemistry and Plasma Processing 28/2 (2008) 289.
[24] T. Jacobs, N. De Geyter, R. Morent, S. Van Vlierberghe, P. Dubruel, C. Leys, Plasma modification of PET foils with different crystallinity,Surface and Coatings Technology 205, Supplement 2/0 (2011) S511.
[25] R. Morent, N. De Geyter, X.D. Zhang, T. Gamblicher, B. Xu, S. Gaan, V. Salimova, P. Rupper, J. Hu, M. Q., S. Mondal, J. Dyer, J.R. Owens, N. Pan, J.V. Edwards, S. Goheen, H.J. Lee, G. Sun, D. Hayes, S. Obendorf, functional textiles for improved performance, protection and health, Woodhead publishing, 2011.
[26] P.L. Girard-Lauriault, P. Desjardins, W.E.S. Unger, A. Lippitz, M.R. Wertheimer, Chemical characterisation of nitrogen-rich plasma-polymer films deposited in dielectric barrier discharges at atmospheric pressure,Plasma Process Polym 5/7 (2008) 631.
[27] P. Heyse, R. Dams, S. Paulussen, K. Houthofd, K. Janssen, P.A. Jacobs, B.F. Sels, Dielectric barrier discharge at atmospheric pressure as a tool to deposit versatile organic coatings at moderate power input,Plasma Process Polym 4/2 (2007) 145.
[28] H.E. Wagner, R. Brandenburg, K.V. Kozlov, A. Sonnenfeld, P. Michel, J.F. Behnke, The barrier discharge: basic properties and applications to surface treatment,Vacuum 71/3 (2003) 417.
[29] G. Borcia, C. Anderson, N. Brown, Dielectric barrier discharge for surface treatment: application to selected polymers in film and fibre form,Plasma Sources Science and Technology 12/3 (2003) 335.
[30] C. Liu, N. Cui, N. Brown, B.J. Meenan, Effects of DBD plasma operating parameters on the polymer surface modification,Surface and Coatings Technology 185/2 (2004) 311.
[31] C. Liu, J. Wu, L. Ren, J. Tong, J. Li, N. Cui, N. Brown, B. Meenan, Comparative study on the effect of RF and DBD plasma treatment on PTFE surface modification,Materials Chemistry and Physics 85/2 (2004) 340.
[32] A. Marmur, Soft contact: measurement and interpretation of contact angles,Soft Matter 2/1 (2006) 12.
[33] R.N. Wenzel, Resistance of solid surfaces to wetting by water,Industrial & Engineering Chemistry 28/8 (1936) 988.
[34] M. Gazicki, H. Yasuda, An atomic aspect of plasma polymerization: the role of elemental composition of the monomer,Journal of Applied Polymer Science Applied polymer symposium 38 (1984).
[35] J.M. Kelly, R.D. Short, M.R. Alexander, Experimental evidence of a relationship between monomer plasma residence time and carboxyl group retention in acrylic acid plasma polymers,Polymer 44/11 (2003) 3173.
[36] T.B. Casserly, K.K. Gleason, Effect of Substrate Temperature on the Plasma Polymerization of Poly(methyl methacrylate),Chemical Vapor Deposition 12/1 (2006) 59.

Table I: Discharge power for all gasses and conditions used

Plasma gas	**Discharge power (W)**	**Treatment time (sec)**	**Energy Density (J/cm^2)**
Ar	1.12	0-60	0-2.02
He	0.85	0-80	0-2.05
Air	2.00	0-40	0-2.11
N_2	1.85	0-40	0-1.95
He (polymerization)	30.2	60-300	92.28-461.42

Table II: Saturation points used for further analysis

Plasma gas	**Contact angle (°)**	**Energy density (J/cm^2)**	**R(q) (nm)**
Ar	49	1.34	73.5 +/- 13.0
He	62	0.60	57.0 +/- 16.4
Air	55	1.51	55.6 +/- 4.4
N_2	43	1.43	71.2 +/- 14.7
Untreated	93	0	108 +/- 10.1

Table III: Elemental composition and C1s Curve fit results after plasma activation

Plasma gas	**Atomic concentration (%)**			**C1s curve fit (%)**			
	C	O	N	C-C	C-O	C=O	O-C=O
Ar	78.9	21.1	/	88.3	6.3	2.3	3.1
He	84.5	15.5	/	89.0	7.3	1.7	2.0
Air	80.6	19.3	/	88.9	5.9	0.90	4.2
N_2	75.4	17.7	6.9	*	*	*	*

* unable to quantify due to overlap of the deconvoluted peaks caused by limited spatial resolution

Table IV: WCA and XPS results for PMMA plasma deposited film

Treatment time	**WCA (°)**	**O/C ratio**	**C1s curve fit (%)**			
			C-C	C-C=O	C-O	O=C-O
50 ml/min						
2	95.2	0.20	81.7	4.6	8.3	5.4
3	75.9	0.22	75.9	8.6	9.1	6.4
4	79.1	0.20	79.2	6.8	8.5	5.5
75 ml/min						
2	85.8	0.24	78.0	5.9	9.3	6.8
3	81.0	0.23	77.6	6.9	8.8	6.6
4	79.5	0.22	78.4	7.7	7.9	6.0
100 ml/min						
2	75.9	0.25	75.5	7.4	9.4	7.7
3	78.5	0.22	79.5	5.3	8.8	6.4
4	79.8	0.24	78.3	6.3	8.7	6.7
125 ml/min						
2	79.0	0.17	79.9	11.1	6.1	3.0
3	76.9	0.19	80.2	7.0	8.0	4.9
4	77.1	0.22	82.7	2.9	9.6	4.9
Commercial	70.0	0.38	59.0	13.7	13.6	13.7

Figure Captions

Figure 1: Schematic representation of the DBD plasma activation reactor (1: gass bottle; 2: Mass flow controller; 3: DBD plate reactor; 4: manometer; 5: pressure valve 6: Oil pump)

Figure 2: schematic representation of the DBD plasma polymerization reactor (1: gass bottle; 2: Mass flow controller; 3: Glass bubbler; 4: DBD plate reactor; 5: manometer; 6: pressure valve; 7: Oil pump)

Figure 3: Voltage - current plots of Ar (a); He (b); air (c) and N_2 (d) respectively for the plasma activation and the voltage current plot of He (e) for the plasma polymerization

Figure 4: Contact angle measurements for plasma activated UHMWPE in function of energy density for Ar, He, air and N_2.

Figure 5: General representation of a C1s curve fit for plasma activated UHMWPE (up) and PMMA (down)

Figure 6: Series of AFM images showing from them from left to right in function of treatment time (1-5 min) and from top to bottom in function of monomer flow rate (50-125 ml/min).

Figure 7: Thickness of the deposited Plasma PMMA films as a function of treatment time for three different monomer flow rates (75-100-125 ml/min)

Figure 8: FT-IR spectrum of untreated UHMWPE

Figure 9: FT-IR spectra of (a) plasma polymerized PMMA deposited on UHMWPE substrate in function of time (b) plasma polymerized PMMA samples after 2 weeks of incubation (c) different incubation times of the 100ml/min-3min condition

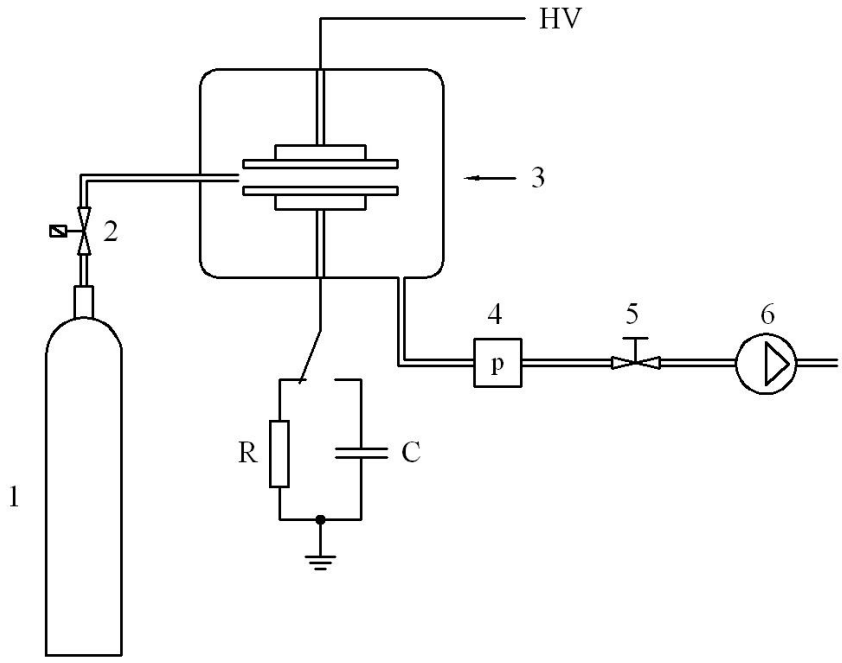

Figure 1

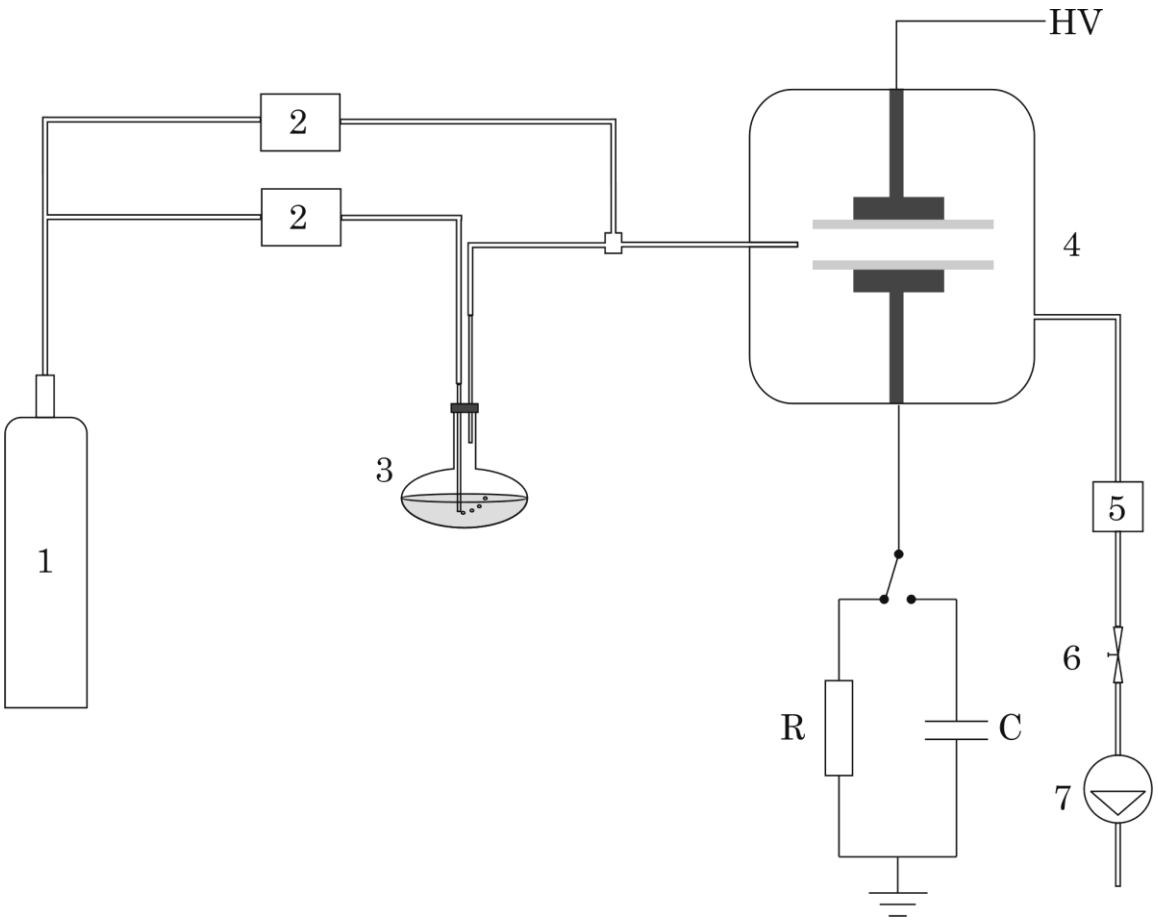

Figure 2

Figure 3

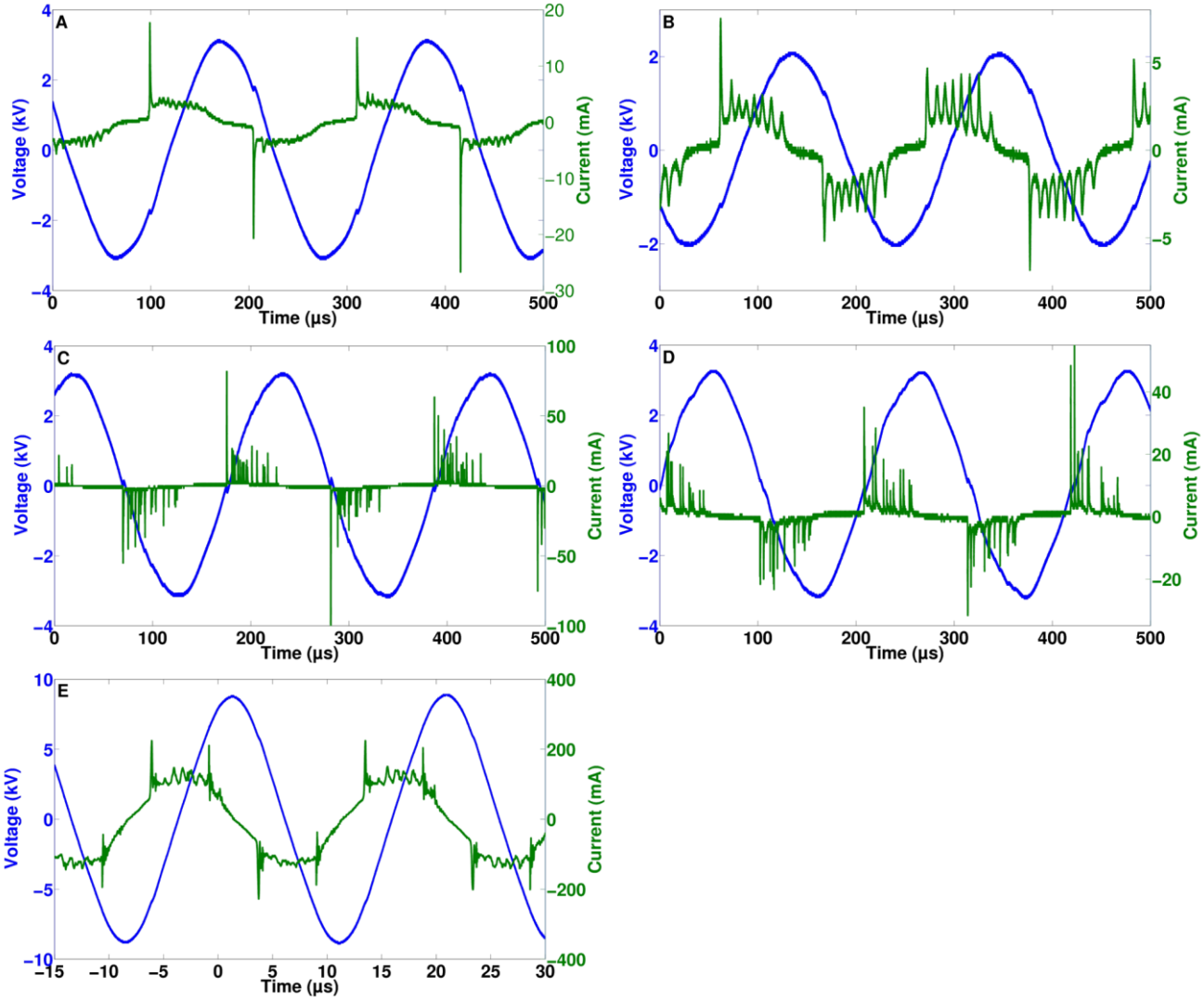

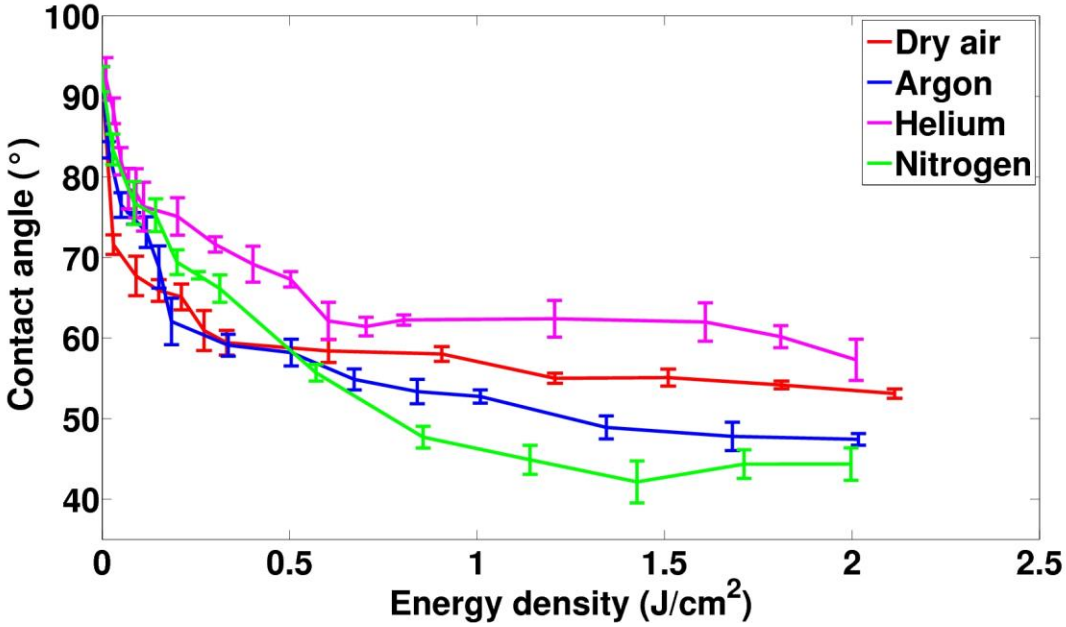
Dry air
Argon
Helium
Nitrogen
Contact angle (°)
Energy density (J/cm2)
100
90
80
70
60
50
40
0
0.5
1
1.5
2
2.5

Figure 4

Figure 5

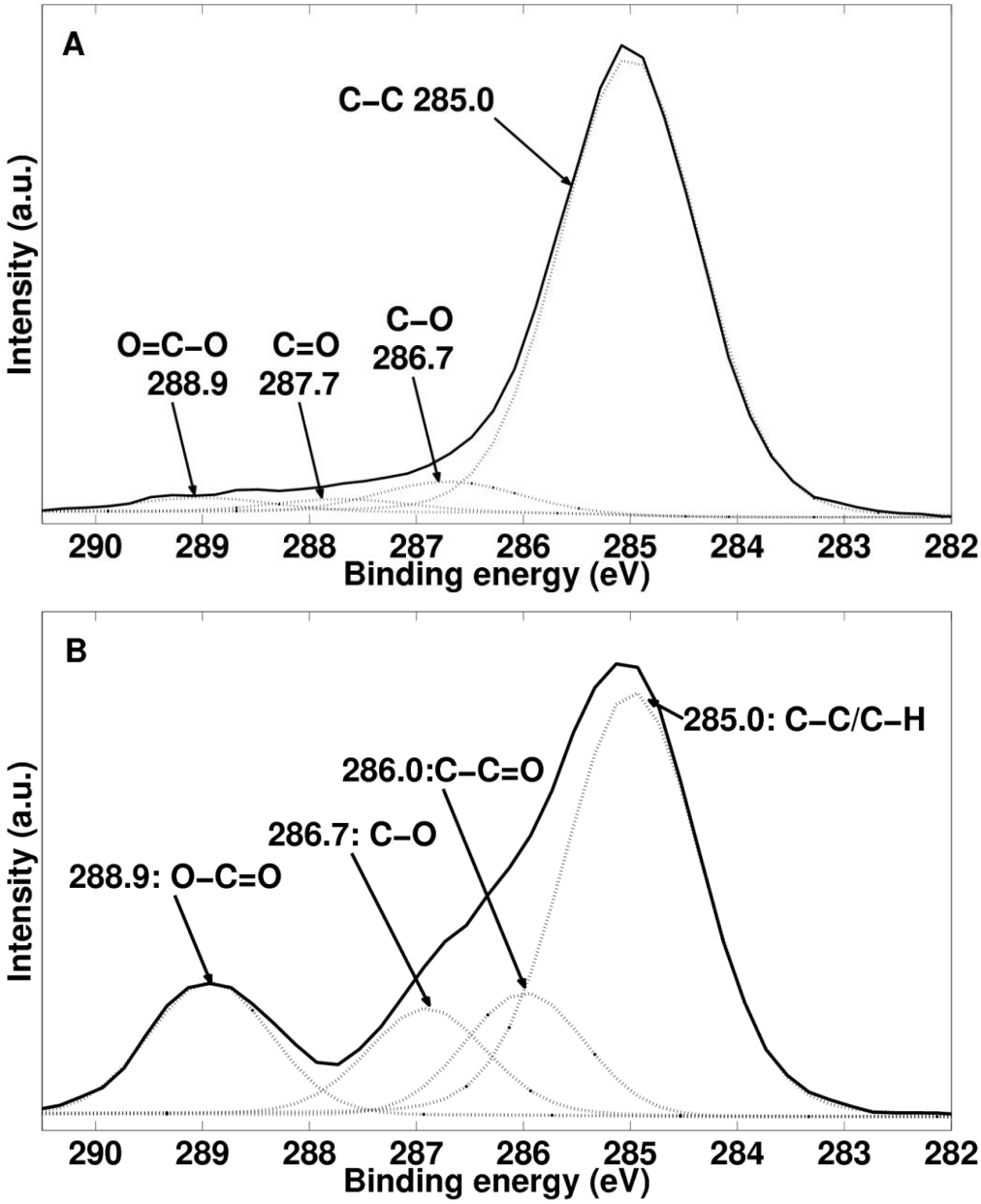
A
C–C 285.0
O=C–O
288.9
C=O
287.7
C–O
286.7
Intensity (a.u.)
290
289
288
287
286
285
284
283
282
Binding energy (eV)
B
285.0: C–C/C–H
286.0:C–C=O
286.7: C–O
288.9: O–C=O
Intensity (a.u.)
290
289
288
287
286
285
284
283
282
Binding energy (eV)

Figure 6

ml/ min	1 min	3 min	5 min
0		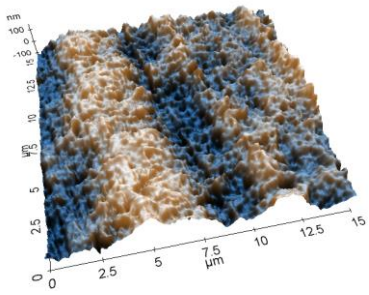	
50	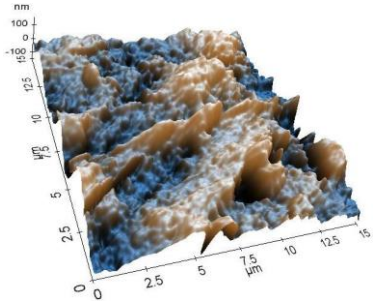	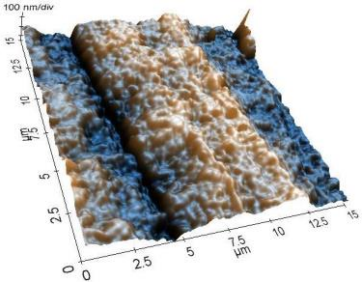	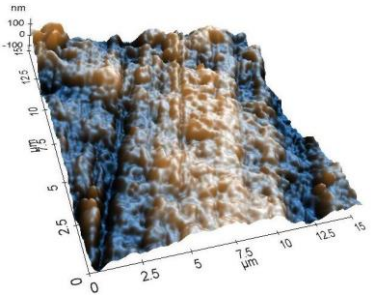
75	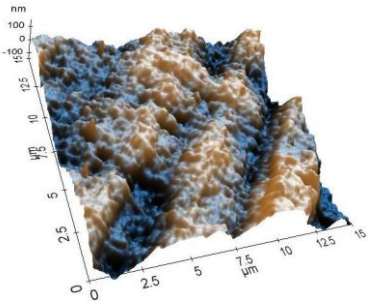	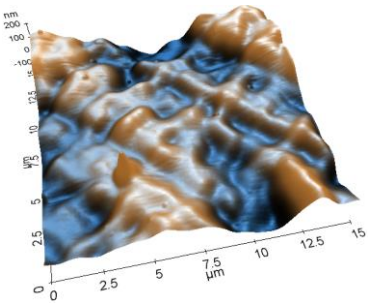	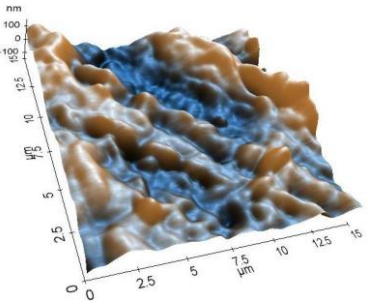
100	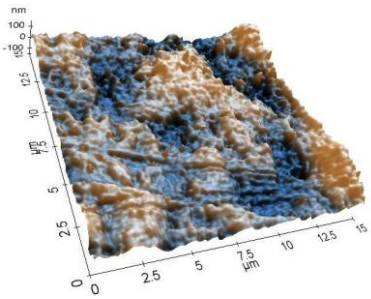	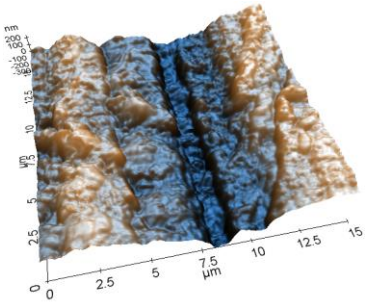	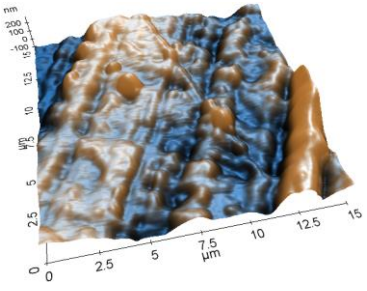

125	

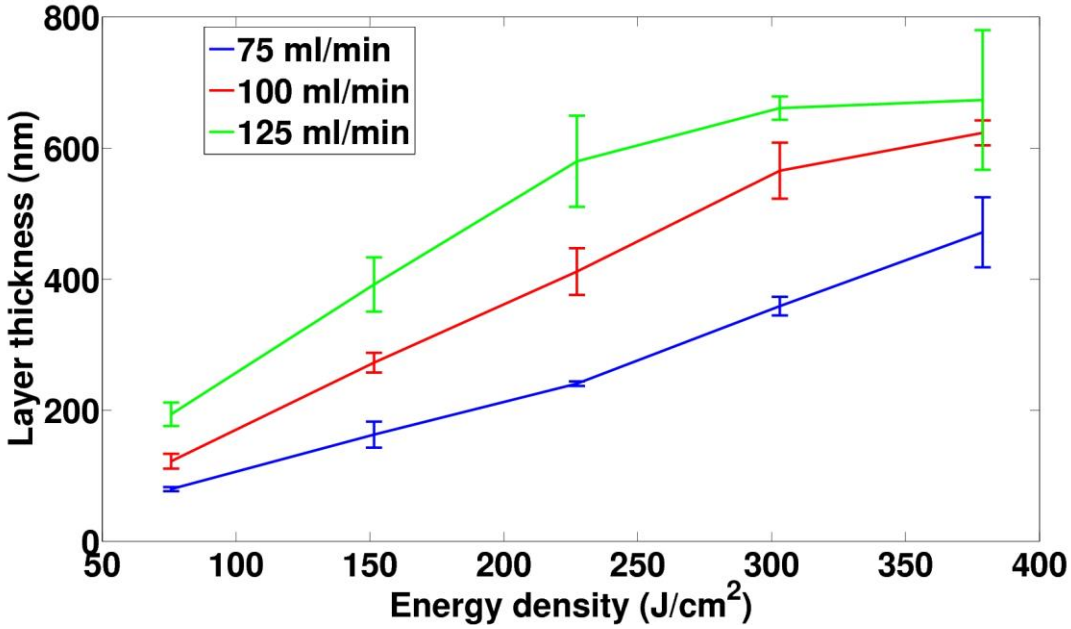
75 ml/min
100 ml/min
125 ml/min
Layer thickness (nm)
Energy density (J/cm2)
0
200
400
600
800
50
100
150
200
250
300
350
400

Figure 7

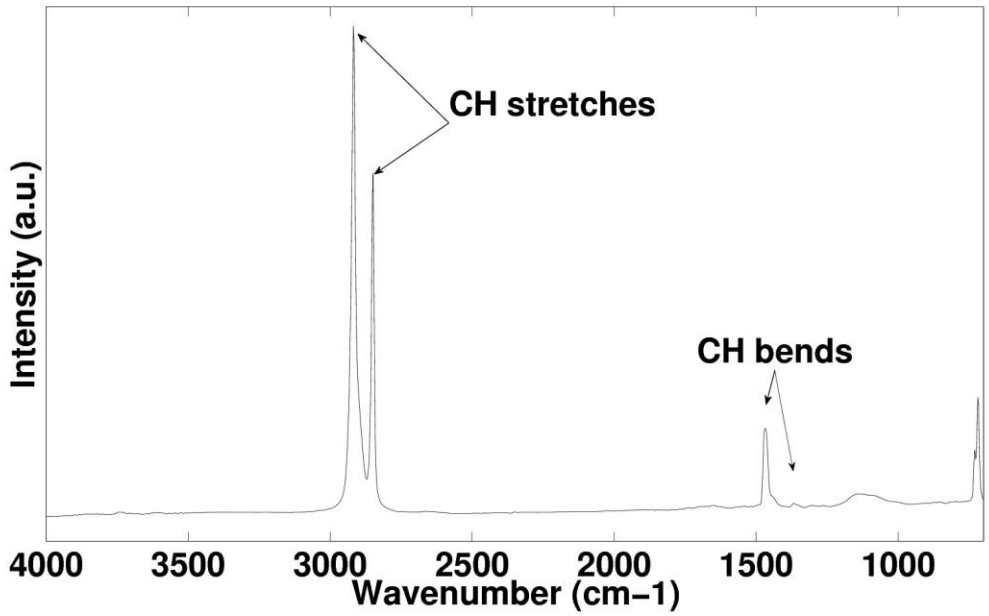
CH stretches
CH bends
Intensity (a.u.)
4000
3500
3000
2500
2000
1500
1000
Wavenumber (cm−1)

Figure 8

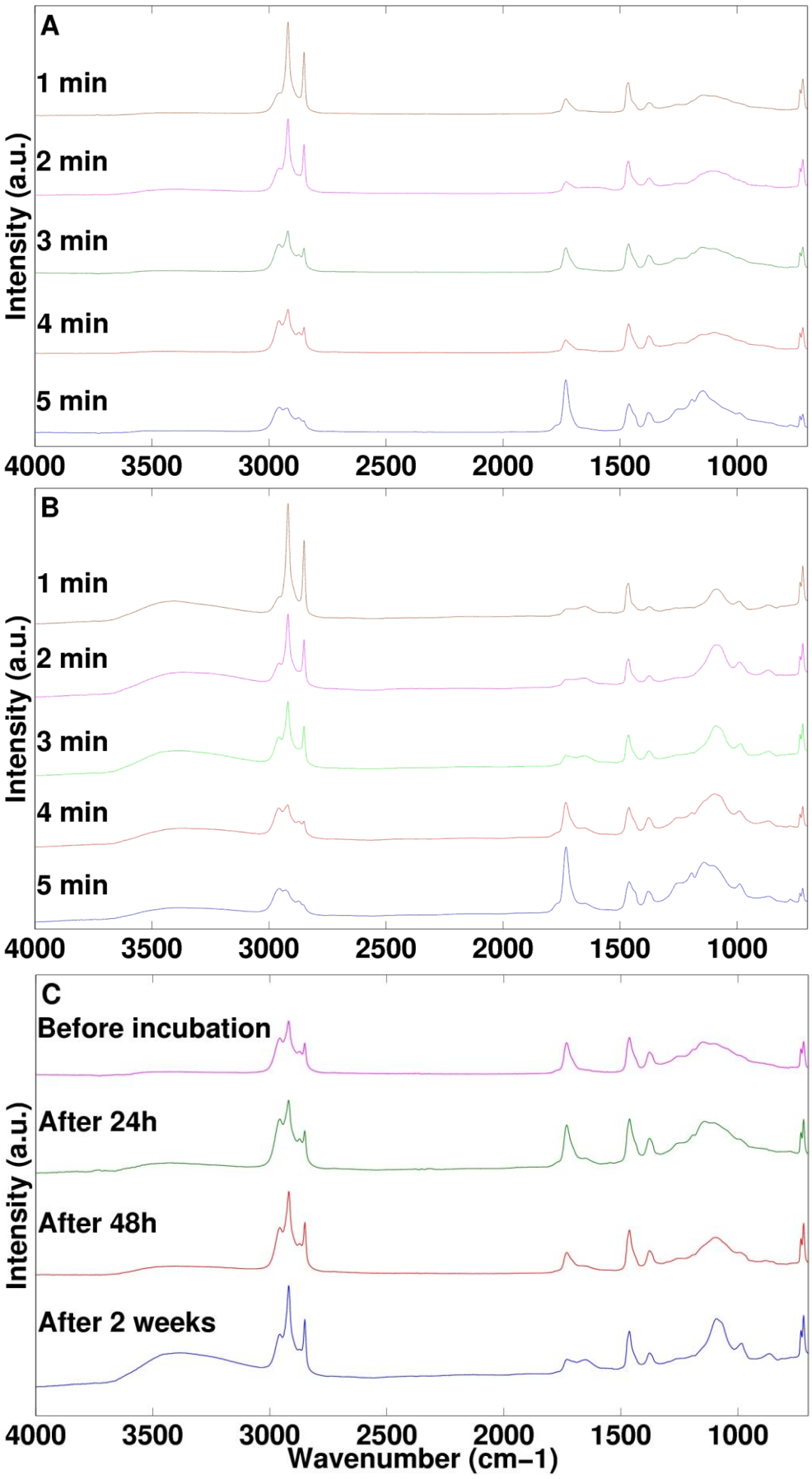
A
1 min
2 min
3 min
4 min
5 min
Intensity (a.u.)
4000
3500
3000
2500
2000
1500
1000
B
1 min
2 min
3 min
4 min
5 min
Intensity (a.u.)
4000
3500
3000
2500
2000
1500
1000
C
Before incubation
After 24h
After 48h
After 2 weeks
Intensity (a.u.)
4000
3500
3000
2500
2000
1500
1000
Wavenumber (cm−1)

Figure 9